Available online at www.sciencedirect.com
ScienceDirect
Optics Communications 265 (2006) 494–499
OPTICS COMMUNICATIONS
www.elsevier.com/locate/optcom

Distributed temperature measurement using a Fabry–Perot effect based chirped fiber Bragg grating

P.C. Won *, Y. Lai, W. Zhang, J.S. Leng, J.A.R. Williams

Photonics Research Group, Aston University, Aston Triangle, Birmingham B4 7ET, United Kingdom

Received 7 March 2005; received in revised form 3 April 2006; accepted 8 April 2006

Abstract

A temperature distribution sensing system based on the reflection spectrum of a 70 mm apodized chirped fiber Bragg grating has been demonstrated. Reflection variations created by the Fabry–Perot effect due to the intra-grating wavelength shift are presented. By fitting a parametric transfer matrix model of the grating response to measured spectra, the temperature change, position and width of a localized temperature change are obtained. This system is particularly attractive of its simplicity, high spatial resolution and ability in measuring a non-monotonic distribution. Experiments to measure two localized heating regions along the grating indicate that the technique is promising for measuring more complex temperature profiles.

Keywords: Fiber-optic sensors; Temperature measurement; Bragg grating

1. Introduction

The use of fiber Bragg gratings (FBGs) in sensing applications is becoming more important due to their advantageous properties such as immunity to electromagnetic fields and sensitivity to disturbances such as strain, temperature, pressure and vibration. To date, there have been many reported methods of Bragg grating based distributed sensing [1–8]. Many of these schemes are restricted to measuring a monotonically changing distributed perturbation [1–4]. Some require the setup of interferometric [1,3] or radio frequency schemes [4] that are often complex and costly for on-site application. On the other hand, it is interesting to note in [5–8] that genetic algorithm approach and time–frequency signal analysis have been proposed to reconstruct a non-monotonic strain distribution based on the reflection spectrum of gratings. The numerical simulations have successfully shown the potential and versatility of these approaches despite there exist possible problems induced by the dependence of initial values in the proposed algorithms.

In this paper, we demonstrate a distributed temperature sensing system consisting of an apodized chirped fiber grating. A least squares fitting process is adopted together with the standard "Rouards" method for calculating Bragg grating spectra in order to obtain the temperature change, position and width of a localized region of heating. Experiments with one and two heating regions have been carried out showing that the system is capable in providing distributed measurements.

2. Background

When grating is heated, its Bragg wavelength shifts from its original wavelength to a wavelength with a higher value. For a chirped FBG, the localized heating within grating manifests itself as a localized shift in the resonant wavelength of the grating. This localized resonant wavelength shift causes two separate regions in the grating being resonant at the same wavelength leading to the formation of Fabry–Perot (FP) cavities within the chirped grating. This phenomenon is illustrated in Fig. 1, in which the

* Corresponding author. Tel.: +44 1212043519; fax: +44 1212053682.
E-mail addresses: wonpc@aston.ac.uk, p.c.won@aston.ac.uk (P.C. Won).

0030-4018/$ - see front matter © 2006 Elsevier B.V. All rights reserved.
doi:10.1016/j.optcom.2006.04.024

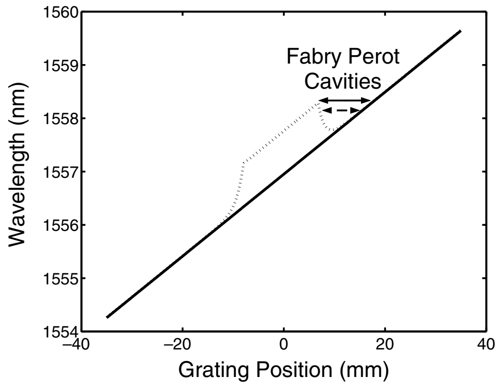

Fig. 1. Resonant wavelength distributions at $\Delta T = 0$ K (—) and $\Delta T = 60$ K (···) along a chirped FBG.

wavelength distribution of a grating with single heated region at $\Delta T = 60$ K is shown. The same concept applies to multiple localized heating regions. As an example, the wavelength distribution for two localized heat regions at $\Delta T = 50$ K is shown in Fig. 2.

As can be seen from both figures, grating is interrupted due to the intra-grating wavelength shift. This shift reduces the reflectivity of the original wavelength corresponding to the heating location and forms FP cavities at the higher resonant wavelength. Consequently, the reflectivity of the grating wavelength at the new resonant wavelength is increased due to the resulted FP resonant cavities. The free spectral range of the FP cavities produced in the grating depends on the magnitude of the resonant wavelength shift, which in turn, depends on the magnitude of temperature change. This FP effect plays an important role because it causes significant reflectivity variation within the grating which serves as useful information of the spatial distribution of the temperature change.

3. Parametric model

There are many simulation techniques for FBGs, for instance, numerical integration of coupled-mode equations, and Rouard's transfer matrix technique. Among them, transfer matrix method is fast and straightforward, and therefore it is extensively implemented. In this method, coupled mode equations are used to calculate the output fields of a short section δl_1 of grating for which the grating length L_g, the coupling constant $\kappa(z)$ and chirp $\gamma(z)$ are assumed to be constant. Each may possess a unique and independent functional dependence on the spatial parameter z. For such a grating with an integral number of periods, the analytical solution results in the amplitude reflectivity, transmission and phase. These quantities are then used as the input parameters for the adjacent section of grating of length δl_2 [9].

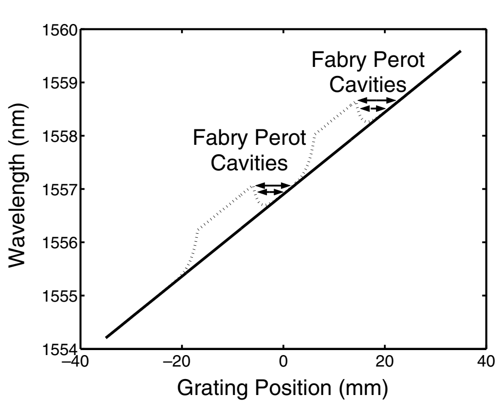

Fig. 2. Resonant Wavelength distribution at $\Delta T = 0$ K (—) and resonant wavelength distributions of two heated regions at $\Delta T = 50$ K (···) along a chirped FBG.

For distributed temperature sensing using nth hyper-Gaussian apodized chirped fiber grating, the position z-dependent coupling constant, $\kappa(z)$, and Bragg wavelength, $\lambda_B(z)$, functions can be defined as;

$$\kappa(z) = \kappa \exp\left[-\left(\frac{z}{l/2}\right)^{2n} \log 2\right] \tag{1}$$

$$\lambda_B(z) = \lambda_c + \gamma z + g(z, \Delta T, L_p, C_p) \tag{2}$$

where κ is the coupling constant and the exponential function in $\kappa(z)$ is a nth-order hyper-Gaussian apodized profile applied during grating fabrication. l is the physical length of grating at 3 dB bandwidth, λ_c is the central wavelength of grating, γ is the effective chirp rate and $g(z, \Delta T, L_p, C_p)$ is the temperature profile along the grating under test with ΔT is the applied temperature change, L_p is the width and C_p is the position of the heat source with reference to the center of the grating.

In this paper, for illustrative purposes, a known temperature change profile is applied to the chirped grating using three contiguous peltiers. When the central peltier acts as the heat source with the rest remain at the room temperature, the temperature change profile can be modelled using the function;

$$g(z, \Delta T, L_p, C_p) = \begin{cases} A\Delta T \exp(k_1(z-a)) & \text{if } z < a \text{ with } a = C_p - 0.5L_p \\ A\Delta T & \text{if } b < z < a \\ A\Delta T \exp(k_2(b-z)) & \text{if } z > b \text{ with } b = C_p + 0.5L_p \end{cases} \tag{3}$$

where A is the temperature dependent coefficient of the grating, k_1 and k_2 are the temperature decay coefficients of the function that depend on the ΔT and account for the heat flow into the areas adjacent to the heat source. In this work, with the same physical conditions at either side of the heated region, we can assume $k = k_1 = k_2$.

4. Data fitting

By using the proposed parametric model of the temperature profile applied on the grating, we can determine the grating structure and calculate the resulted reflectivity spectrum based on the transfer matrix method. The parameters in the model are adjusted to least squares fit the calculated spectrum to the experimentally measured spectrum. By optimizing the values of the parameters, we can determine the applied temperature ΔT, position C_p and width L_p of the applied heat, and the appropriate terms to account for the heat flow of each specific experimental configuration.

Before determining the ΔT, C_p and L_p of the perturbed gratings, the reflection spectrum of the unperturbed case (with $\Delta T = 0$ K) is first recorded and used as the experimental reference reflection spectrum. A fitting is made to this spectrum in order to identify the imprecisely known grating parameters, which are κ, γ, full width at half maximum (FWHM) bandwidth and the central frequency of the grating. This measurement is only made once and is used to characterize the grating before it is used as a sensor.

Based on the grating parameters of the unperturbed grating, the calculated reflection spectrum with the effect of temperature change profile $g(z, \Delta T, L_p, C_p)$ is least squares fitted to the experimental reflection spectrum with temperature change. Fitting process stops only when the desired fitness is achieved, in which the fittest values of ΔT, C_p and L_p are obtained. On a typical desktop computer, the process takes several minutes to determine the three parameters depending on the desired fitness and number of wavelength points measured on the spectrum. Like other conventional optimization methods [6,8], its performance depends on the number of the unknown parameters and the initial choice of values. Generally, for a slowly varying temperature change, the previous set of values is used as the starting point for the subsequent measurement to enable the tracking of the distributed temperature changes.

5. Experimental setup and results

Fig. 3 shows the experimental setup for the sensing system. A 70 mm chirped grating with 3 dB bandwidth of 2.9 nm was used. The reflection spectrum of the grating was measured using a fast scanning tunable laser and an optical spectrum analyzer. Localized heating was applied to the grating using three contiguous temperature controlled peltiers; P1, P2 and P3 with lengths of 31.5 mm, 15 mm and 70 mm respectively; as shown in Fig. 4. The central peltier P2 was used to apply a known localized temperature change while the outside peltiers P1 and P3 were used to maintain a constant temperature for the remainder of the grating throughout the tests. The peltiers were thermally insulated from each other using a thin mica sheet.

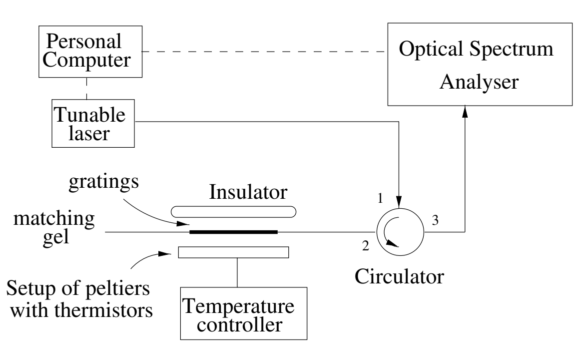

Fig. 3. Schematic diagram of experimental setup.

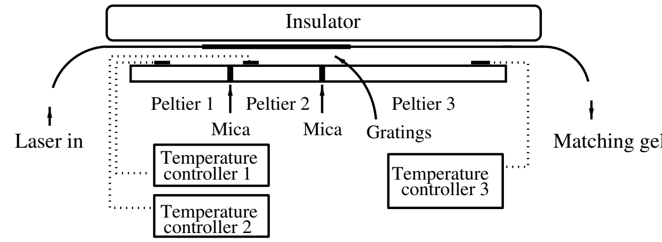

Fig. 4. Schematic diagram of the setup of peltiers.

For illustrative purpose, all three peltiers were placed at known positions with respect to the grating and set to room temperature to obtain the reference reflection spectrum. The temperature of the central peltier P2 was then increased by 60.0 K in steps of 5.0 K. Reflection spectra were recorded and the model spectra fitted at each step. The goodness of fit threshold was set to be 1×10^{-6} for every fit. To provide an idea in how the reflection spectrum changes with the temperature change, Fig. 5 shows the comparison between the reference reflection spectrum and the reflection spectrum obtained with a ΔT of 10 K. It can be seen that there is a significant change in the reflection profile when temperature is changed.

A plot of $A\Delta T$ determined from the fitted model versus the applied temperature change is shown in Fig. 6. We have good agreement to a straight line with a temperature dependent coefficient $A = 13.97$ pm/K, which is in agreement with other FBG sensor experiments [10]. The root-mean-square (RMS) deviation from the linearity was 30 pm.

In the second test, the temperature of P2 was maintained at $\Delta T = 40.0$ K and the grating position was moved by 10 mm in steps of 1 mm to the direction of P3. Examples of the spectra measured and fitted for two different positions are shown in Fig. 7 and the comparison between expected and fitted results for different positions is shown in Fig. 8. There is excellent agreement with a RMS deviation from the applied position of only 0.15 mm.

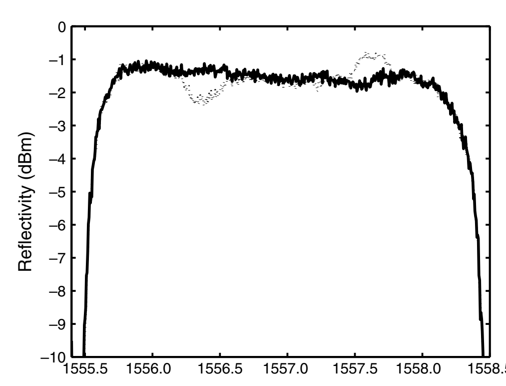

Fig. 5. Reference reflection spectrum (—) and reflection spectrum taken when $\Delta T = 10$ K (···).

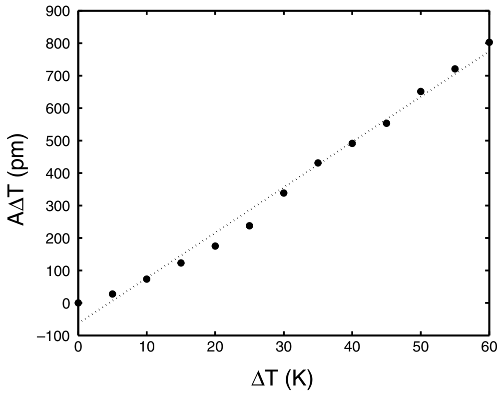

Fig. 6. Fitted $A\Delta T$ (●) versus applied ΔT. Slope (···) gives the temperature dependent coefficient $A = 13.97$ pm/K.

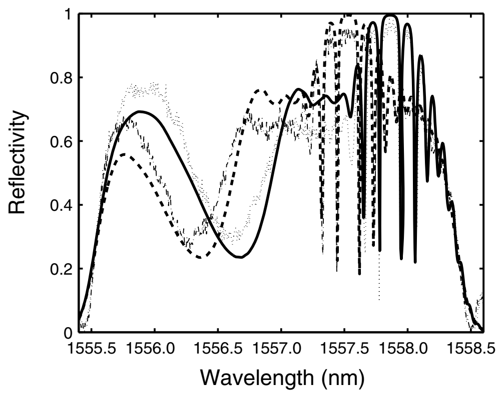

Fig. 7. Experimental (···) and fitted (—) spectra obtained at heating position of −0.5 mm from the center of the grating, and experimental (-··-) and fitted (---) spectra obtained at heating position of −4.5 mm from the center of the gratings at applied temperature of $\Delta T = 40.0$ K.

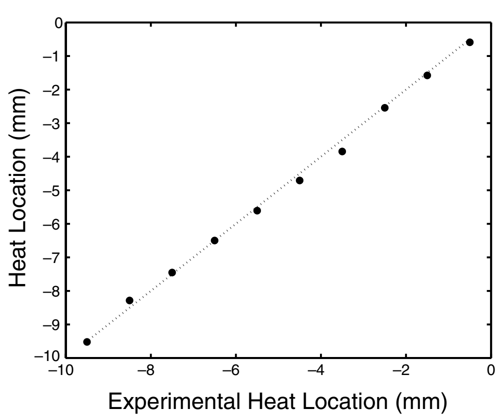

Fig. 8. Expected (···) and fitted (●) results for the determination of position of the heated region.

In the third test, the width of the heated region P2 was varied with ΔT held constant at 30.0 K. Fig. 9 shows the examples of the measured and fitted spectra for two different widths while Fig. 10 shows the comparison between the expected and fitted results. There is, again, excellent agreement with an RMS deviation from the applied width of only 0.31 mm. In repeatability tests, the standard deviations for C_p, L_p and A were obtained as 29 μm, 56 μm

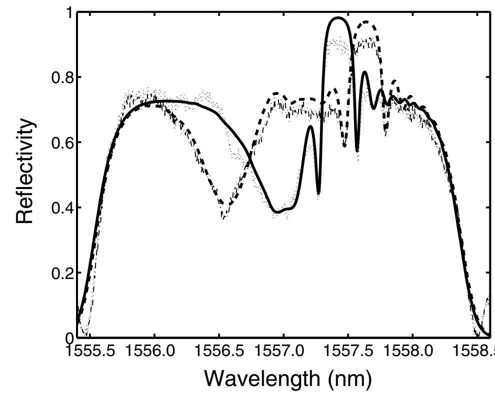

Fig. 9. Experimental (···) and fitted (—) spectra obtained with heating width of 4.0 mm, and experimental (-··-) and fitted (---) spectra obtained with heating width of 12.5 mm at $\Delta T = 30.0$ K.

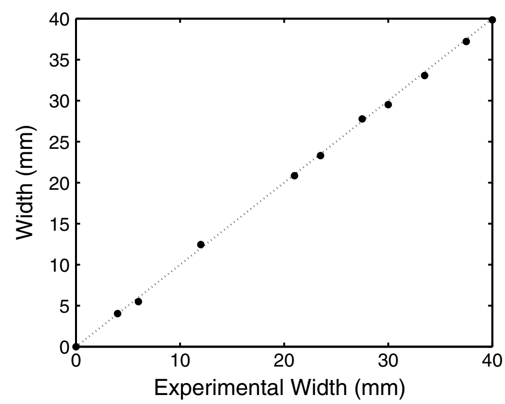

Fig. 10. Expected (···) and fitted (●) results for the determination of width of the heated region.

and 8 pm (corresponding to 0.6 K for ΔT), respectively. Assuming that deviation from linearity is accounted for in making measurements, they correspond to the effective resolutions when the device is used as a sensor.

Finally, in order to show that the system is able to measure distributed temperature change along the grating, an experiment with two regions of elevated temperature was carried out. Fig. 11 shows the experimental and fitted results

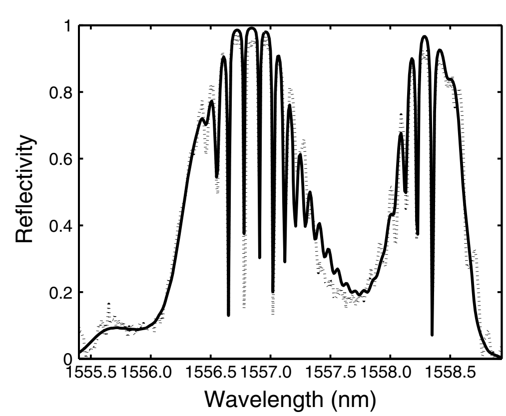

Fig. 11. Experimental (···) and fitted (—) results for two localized heat regions with same temperature change and width but at different positions.

of two heat sources with identical ΔT of 50 K and width L_p of 10 mm at positions C_{p1} and C_{p2} of −12 mm and 10 mm, respectively.

6. Discussion

As can be noticed in Figs. 7 and 9, a number of features arise in the spectrum of the grating which are strongly indicative to the applied temperature profile. These features make the spectrum a good indicator of the applied distributed temperature profile. This scheme has proven to be efficient in characterizing the grating and determining the temperature profile. Experimental results have shown that it is not restricted to a monotonic temperature profile and that it can be used to retrieve temperature profile non-monotonically with high spatial resolution.

Like other optimization methods [6,8], the speed of the least square optimized fitting depends on the number of the unknown parameters, choice of the initial values, desired fitness, number of wavelength measured and the processing speed of the computer in use. These factors are influential and are needed to be well-tailored in order to improve the performance of the process. Alternatively, a simple heuristic way can be used to estimate the initial values. For example, by slowly varying temperature changes, the temperature profile can be estimated by simply using the calculated parameters of the previous measurement.

The maximum temperature that can be measured by this sensing system depends on the bandwidth and the temperature sensitivity of the sensing grating. Since this scheme is based on the Fabry–Perot effect caused by the internal wavelength shift of the grating, it can measure any localized temperature change as long as the resultant resonant wavelength is within the bandwidth of the grating. This condition also ensures that there is no non-linearity in the measurement in the range of measured temperature change. This also implies that when the location of the heat region is further from the edge of the higher wavelength side of the grating bandwidth, the maximum temperature the system can measure is higher than that closer to the edge. It is apparent that temperature sensitivity of the grating also needs to be taken in account for since it affects the internal wavelength shift of grating due to the temperature change. Thus, it is important to characterize the sensing grating prior to the temperature measurement in order to obtain information about its bandwidth and temperature sensitivity.

The proposed system can be tailored for different size of heat source by simply changing the length of the apodized chirped grating. The grating length has to be longer than the heat source if the information of location and width of heat source are of interest in addition to the temperature change. Otherwise, the proposed system can only provide information of the temperature variation based on the wavelength shift as it does in the uniform temperature determination test. However, it is quite difficult to maintain a flat top reflection profile when the length of grating is large since this relies on the stability and alignment of the fabrication apparatus. This situation becomes worse when the grating is made with higher chirp-rate since more stringent alignment is required. Thus, a compromise has to be made in order to reach an optimum balance between the length of grating and the flat top reflectivity in order to have a higher accuracy. In the perfect case, with flat top reflection maintained throughout the bandwidth of gratings, there is no fundamental limitation for the length of the sensing grating.

Nevertheless, as mentioned earlier on, the speed of the fitting process depends on the number of wavelength points scanned. This is due to the fact that the parametric model is based on the implementation of transfer matrix method applied onto the coupled-mode theory. Generally, a longer sensing grating will need longer processing time due to the higher number of wavelength points scanned. It is also worth noting that the number of wavelengths scanned is dependent on the value of chirp-rate; the higher the chirp-rate, the more sections of wavelength needs to be measured, since wider bandwidth needs to be measured and simulated. Thus, longer length of sensing grating can be obtained, but this will be at the cost of having longer fitting processing time.

Owing to the fact that two individual Bragg wavelength functions were used to simulate the reflection spectrum of the sensing grating in the two-heated-region temperature measurement, as shown in Fig. 11, ambiguity caused by the temperature summation will be created in the parametric model if the two heated regions are overlapped onto each other. To avoid this, the two heated regions should remain a minimum distance between each other. For example, in our case, a distance of 3.5 mm is recommended. This problem can be easily solved if a more flexible Bragg wavelength function that takes overlapping of heat regions into account for is used.

7. Conclusions

A fully distributed temperature sensor consisting of a chirped grating has been demonstrated. It has shown that the applied temperature profile to the grating can be determined using the transfer matrix method by means of least squares optimizing the calculated reflection spectrum with the experimental reflection spectrum. Simultaneous determination of the temperature change, position and width of the heat sources can be achieved to a standard deviation of 0.6 K, 29 μm and 56 μm, respectively. Experimental results have proven that this scheme can also be applied to the simultaneous temperature measurement of multiple heat sources.

References

[1] S. Huang, M. Ohn, R. Measures, Applied Optics 35 (1996) 1135.
[2] M. LeBlanc, S. Huang, M. Ohn, R. Measures, Optics Letters 21 (1996) 1405.
[3] M. Ohn, S. Huang, R. Measures, Electronics Letters 33 (1997) 1242.
[4] G. Duck, M. Ohn, Optics Letters 24 (2000) 90.

[5] J. Azana, M.A. Muriel, Optics Letters 25 (2000) 698.
[6] F. Casagrande, P. Crespi, A. Grassi, A. Lulli, R. Kenny, M. Whelan, Applied Optics 41 (2002) 5238.
[7] J. Azana, M.A. Muriel, L.R. Chen, P.W.E. Smith, Journal of Lightwave Technology 19 (2001) 646.
[8] Y-L. Lo, H-C. Cheng, in: Proceedings of the 16th Optical Fiber Sensors Conference Technical Digest (2003) 368.
[9] R. Kashyap, Fiber Bragg gratings, Academic Press, 1999.
[10] A.B.L. Ribeiro, Y.J. Rao, L. Zhang, I. Bennion, D.A. Jackson, Applied Optics 35 (1996) 2267.